Supporting Information

An investigation into support cooperativity for the deoxygenation of guaiacol over nanoparticle Ni and Rh_2P

Michael B. Griffin, Frederick G. Baddour, Susan E. Habas, Connor P. Nash, Daniel A. Ruddy, Joshua A. Schaidle

Guaiacol conversion was calculated according to equation 1, where $\dot{n}_{in,gua}$ and $\dot{n}_{out,gua}$ represent the inlet and outlet molar flow rates of guaiacol, respectively.

$$Conversion = \frac{\dot{n}_{in,gua} - \dot{n}_{out,gua}}{\dot{n}_{in,gua}} * 100\% \quad (1)$$

The product selectivity was calculated separately for the C_5+ products and by-products and each category totals 100%. These calculations were performed using equation 2, where $\dot{n}_i$ represents the molar flow rate of C_5+ product or by-product *i* and $\sum \dot{n}_i$ is the total molar flow rate of either the C_5+ products or the by-products.

$$Selectivity = \frac{\dot{n}_i}{\sum \dot{n}_i} * 100 \quad (2)$$

The H:C ratio was calculated according to equation 3, where $\dot{n}_H$ and $\dot{n}_C$ represent the molar flow rate of hydrogen and carbon contained in the C_5+ products, which excludes unreacted guaiacol.

$$H{:}C\ ratio = \frac{\dot{n}_H}{\dot{n}_C} \quad (3)$$

The average carbon number was calculated according to equation 4, where $\dot{n}_C$ and $\dot{n}_{tot}$ represent the molar flow rate of carbon and the total molar flow rate of the C_5+ products, which excludes unreacted guaiacol.

$$Average\ carbon\ number = \frac{\dot{n}_C}{\sum \dot{n}_{tot}} \quad (4)$$

The C_5+ product yield was calculated according to equation 5, where *X* represents guaiacol conversion, $\dot{n}_i$ represents the molar flow rate of C_5+ product *i*, and $\sum \dot{n}_i$ is the combined molar flow rate of all C_5+ products and by-products.

$$C_5 + product\ yield = X \frac{\dot{n}_i}{\sum \dot{n}_i} \quad (5)$$

The site time yield was calculated according to equation 6, where $\dot{n}_{C5+}$ represents the molar flow rate of all C_5+ products, H^* is H-adsorption site density per gram of Ni or Rh_2P based on H_2 chemisorption analysis of the baseline C-supported catalysts, m_{cat} is the total catalyst mass, and $wt\%_{AP}$ is the active phase loading.

$$Site\ time\ yield = \frac{\dot{n}_{C5+}}{H^* \times m_{cat} \times \frac{wt\%_{AP}}{100}} \tag{6}$$

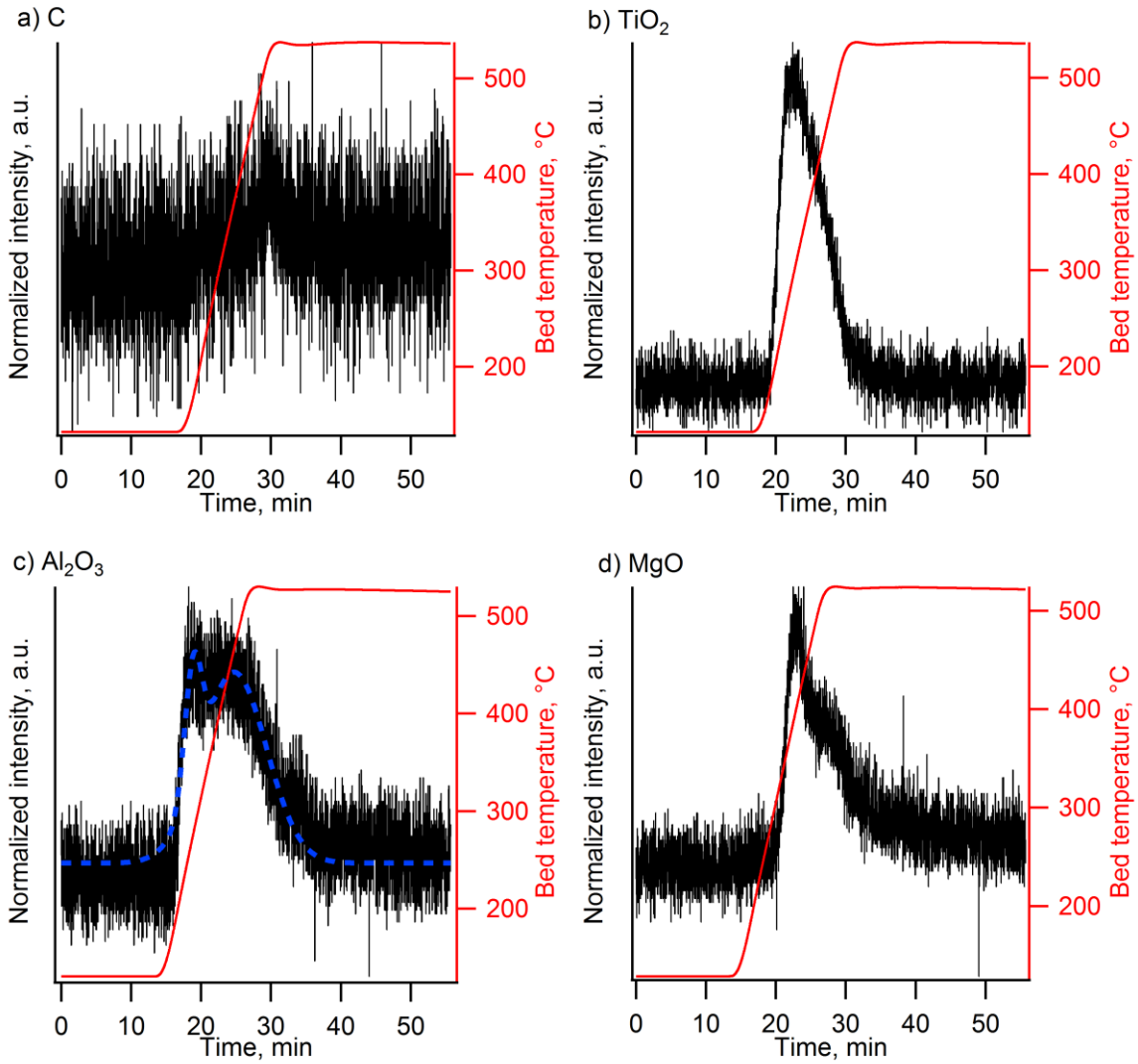

Fig. S1. NH_3-TPD profiles for (a) C, (b) TiO_2, (c) Al_2O_3, and (d) MgO prior to nanoparticle (NP) dispersion. Peak fitting of the Al_2O_3 desorption trace was performed using a Gaussian model and is indicated by the blue dashed line.

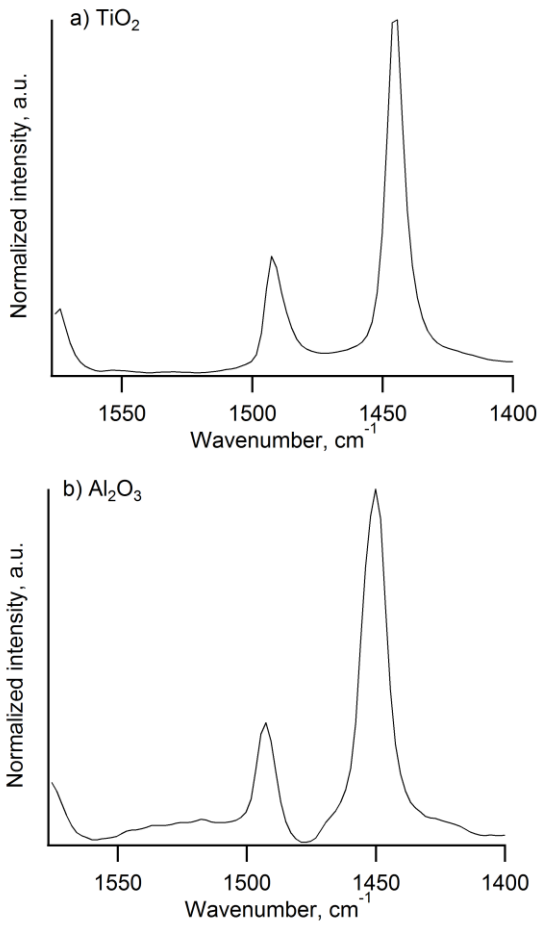

Fig. S2. py-DRIFTS spectra for (a) TiO_2 and (b) Al_2O_3. No pyridine adsorption was detected on C or MgO.

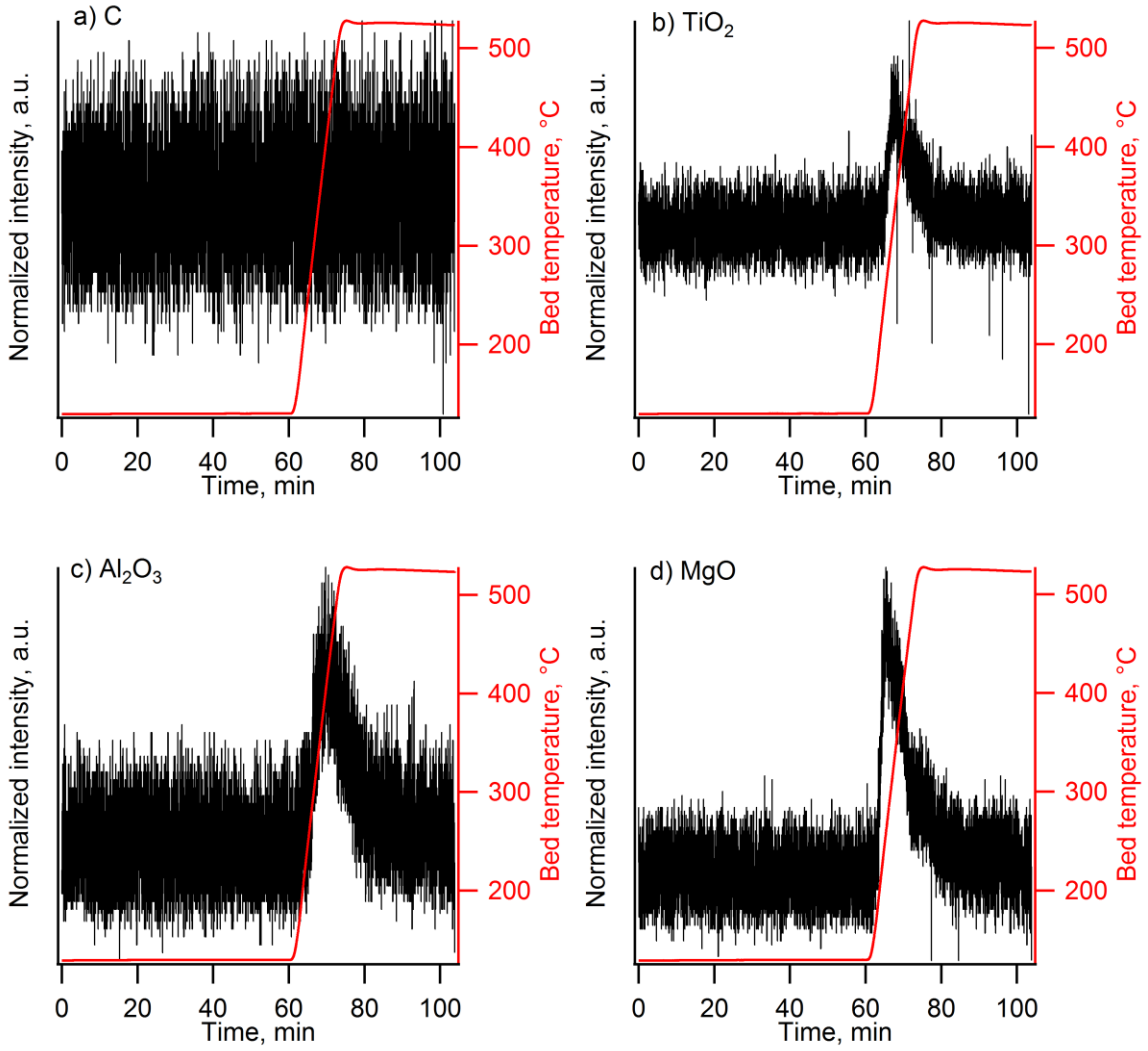

Fig. S3. CO_2-TPD profiles for (a) C, (b) TiO_2, (c) Al_2O_3, and (d) MgO prior to NP dispersion.

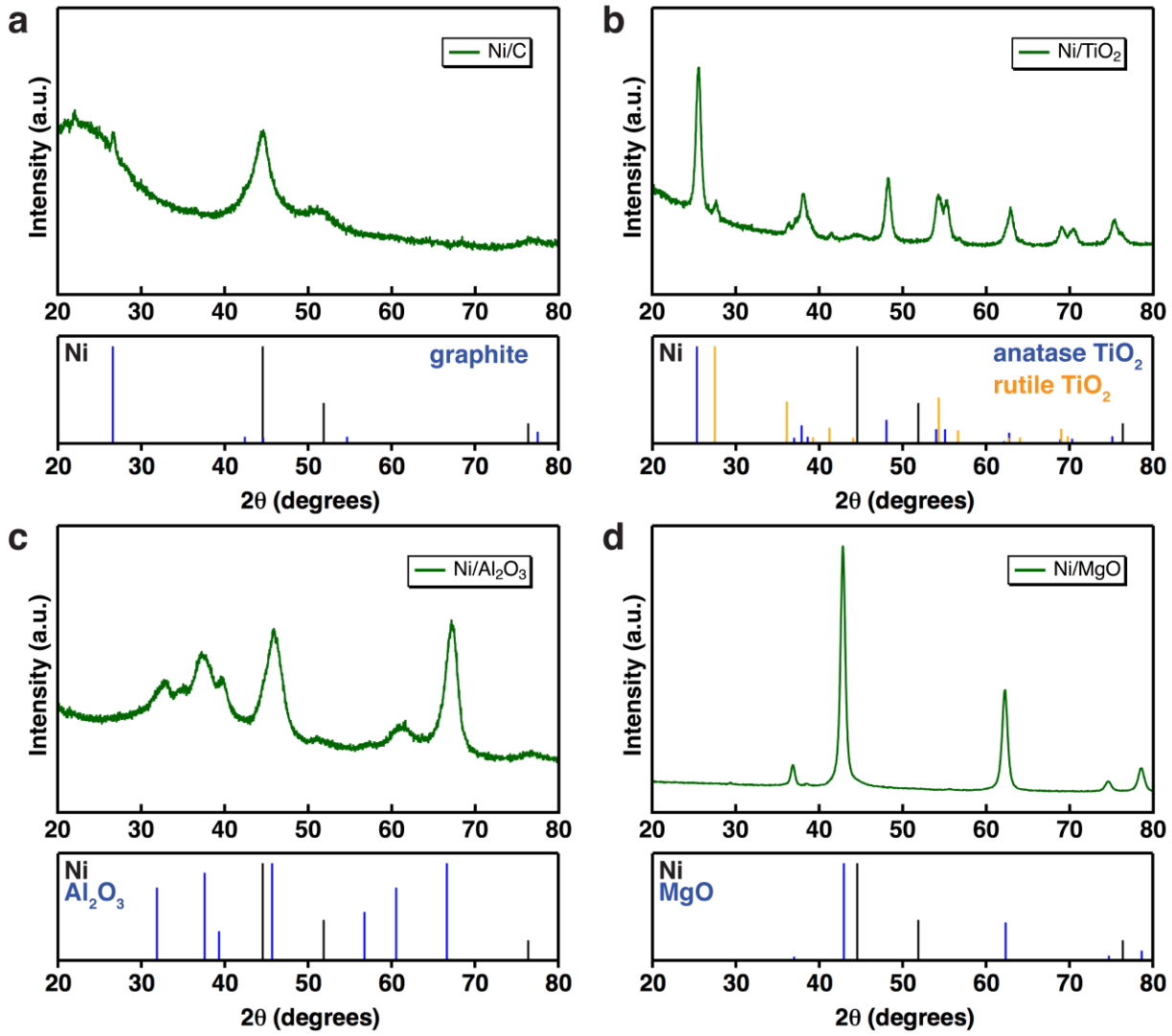

Fig. S4. XRD patterns of (a) Ni/C, (b) Ni/TiO_2, (c) Ni/Al_2O_3, and (d) Ni/MgO prepared by solution NP methods, with reference diffraction patterns.

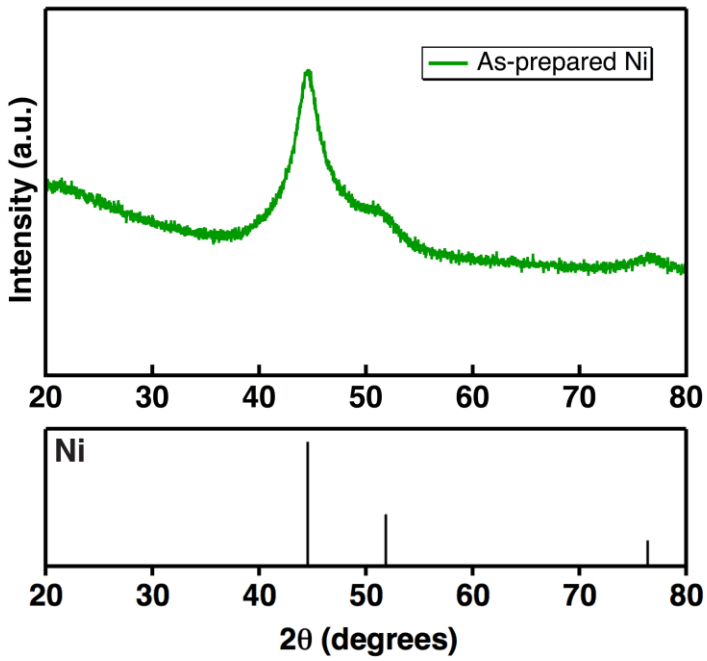

Fig. S5. XRD data and reference pattern of the as-prepared Ni NPs.

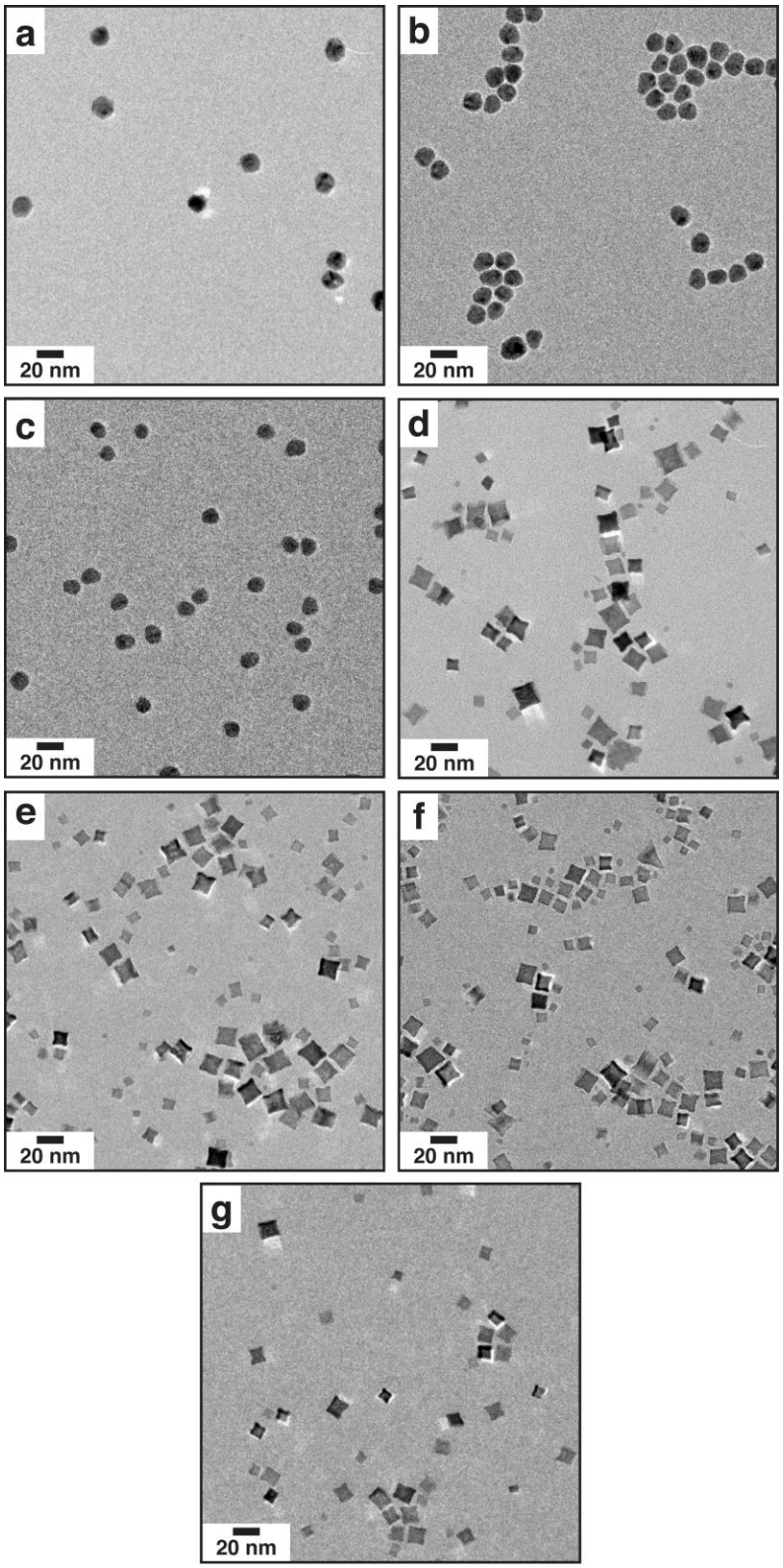

Fig. S6. TEM Images of the as-prepared NPs used to prepare (a) Ni/C, (b) Ni/TiO_2 and Ni/Al_2O_3, (c) Ni/MgO, (d) Rh_2P/C (e) Rh_2P/TiO_2, (f) Rh_2P/Al_2O_3, and (g) Rh_2P/MgO.

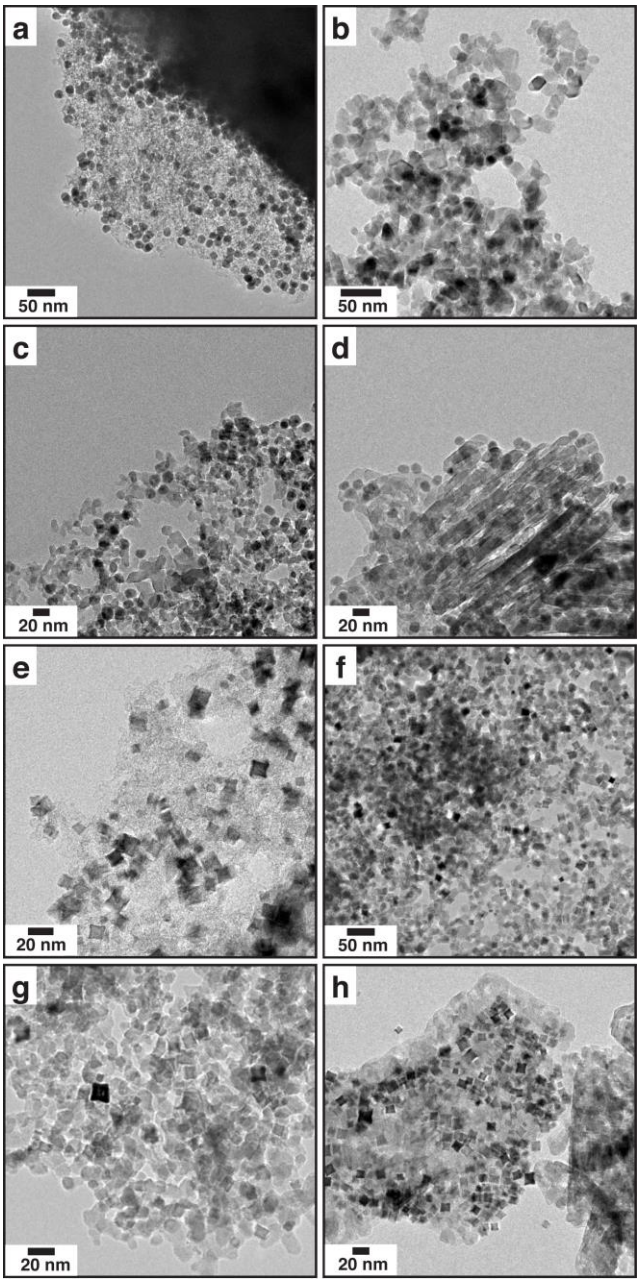

Fig. S7. TEM images of catalysts (a) Ni/C, (b) Ni/TiO_2, (c) Ni/Al_2O_3, (d) Ni/MgO, (e) Rh_2P/C, (f) Rh_2P/TiO_2, (g) Rh_2P/Al_2O_3, and (h) Rh_2P/MgO.

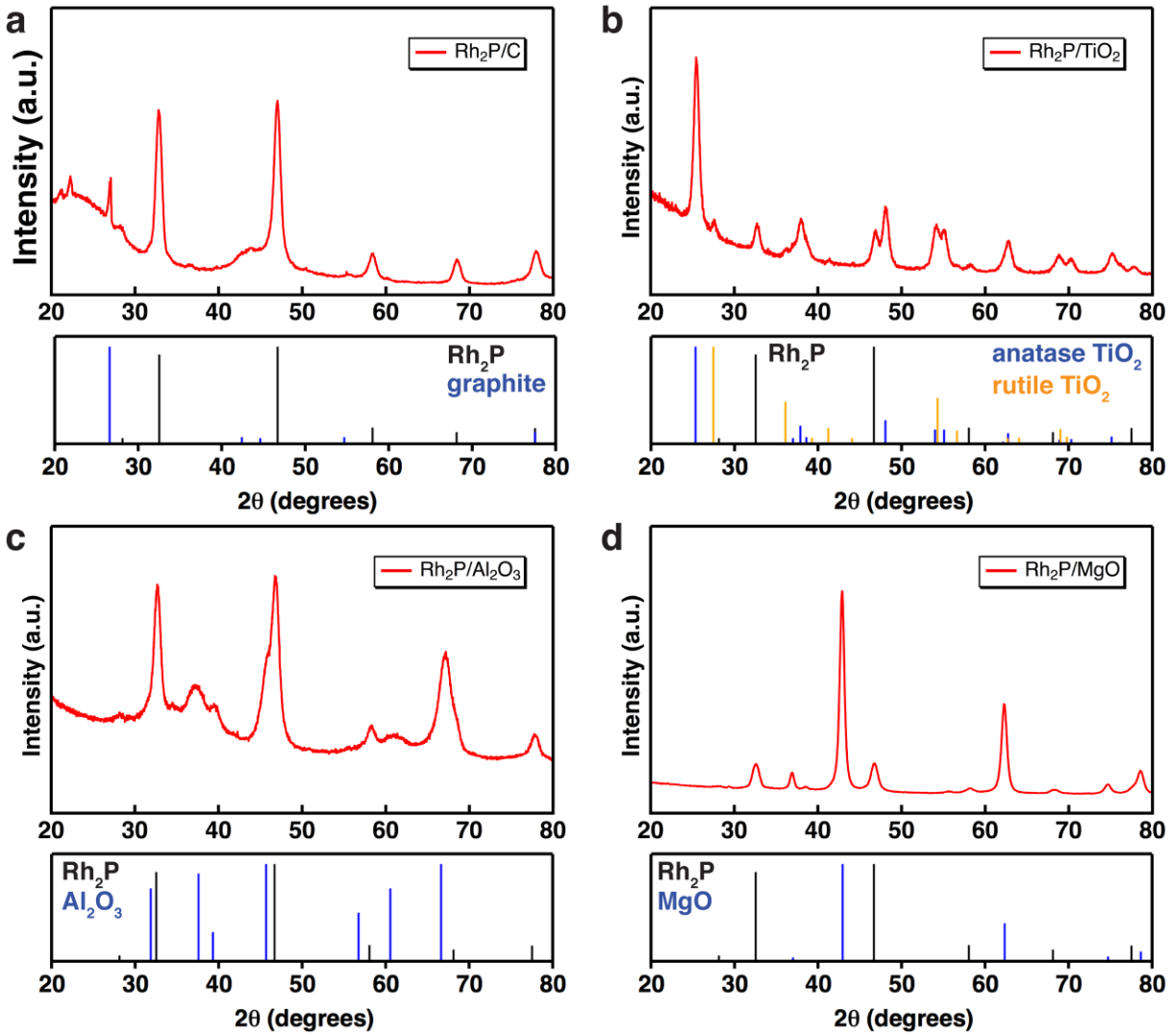

Fig. S8. XRD patterns of supported catalysts (a) Rh_2P/C, (b) Rh_2P/TiO_2, (c) Rh_2P/Al_2O_3, and (d) Rh_2P/MgO prepared by solution NP methods, with reference diffraction patterns.

Table S1: The metal to phosphorus molar ratio of the as-prepared Rh_2P catalysts determined by elemental analysis.

	M:P ratio
Rh_2P/C	1.5
Rh_2P/TiO_2	2.0
Rh_2P/Al_2O_3	1.5
Rh_2P/MgO	1.8

Table S2: Results of methanol and carbon monoxide reactions over Ni/C and Rh_2P/C at 350 °C. Data were collected at 180 ± 20 min time on stream. Reported yields were determined by multiplying the reactant conversion by the product mole fraction.

	Ni/C	Rh_2P/C
	Methanol	
Conversion, %	15.0	4.0
CO Yield, %	14.7	2.6
CH_4 Yield, %	0.3	1.2
	Carbon Monoxide	
Conversion, %	11.9	15.2
CO_2 Yield, %	11.9	0.7
CH_4 Yield, %	-	13.6

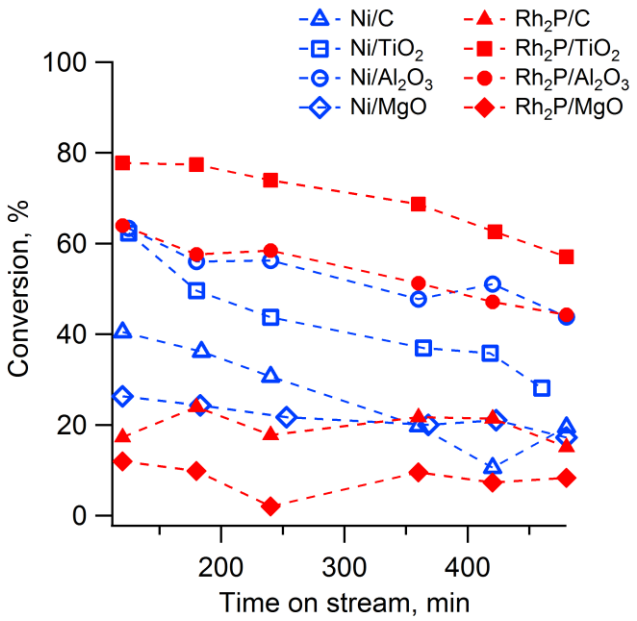

Fig. S9. Conversion as a function of time on stream observed over each catalyst during guaiacol deoxygenation experiments.

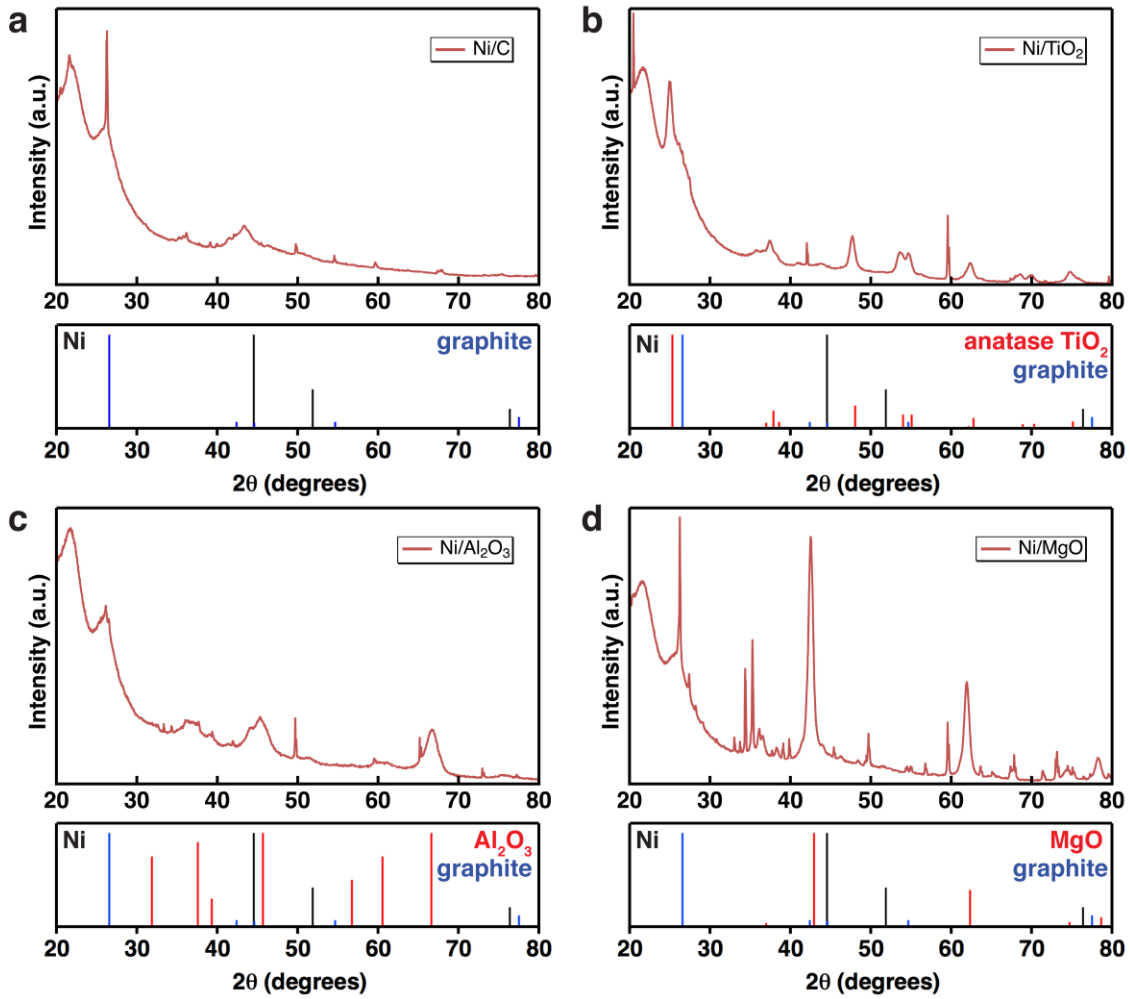

Fig. S10. Post-reaction XRD patterns of (a) Ni/C, (b) Ni/TiO_2, (c) Ni/Al_2O_3, and (d) Ni/MgO prepared by solution NP methods, with reference diffraction patterns.

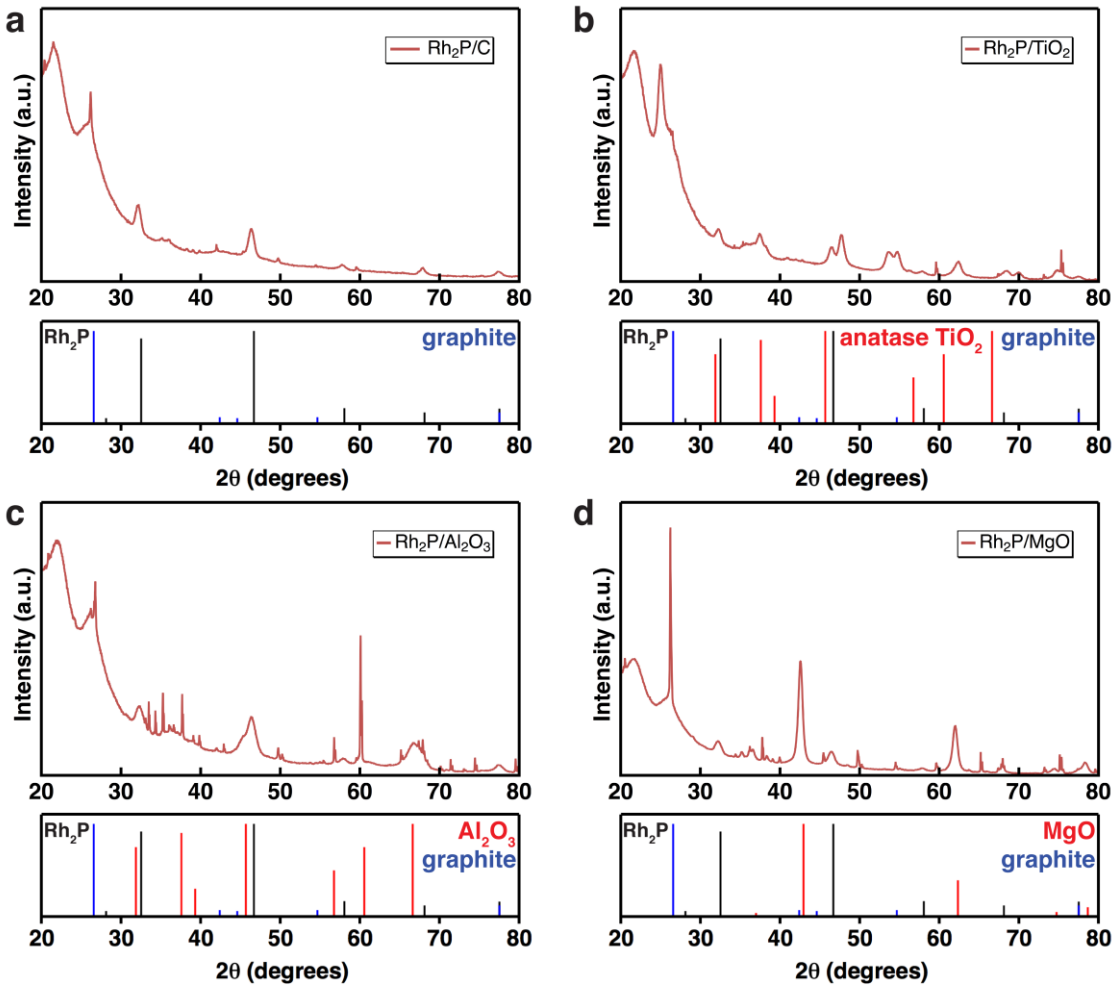

Fig. S11. Post-reaction XRD patterns of catalysts (a) Rh_2P/C, (b) Rh_2P/TiO_2, (c) Rh_2P/Al_2O_3, and (d) Rh_2P/MgO prepared by solution NP methods, with reference diffraction patterns.

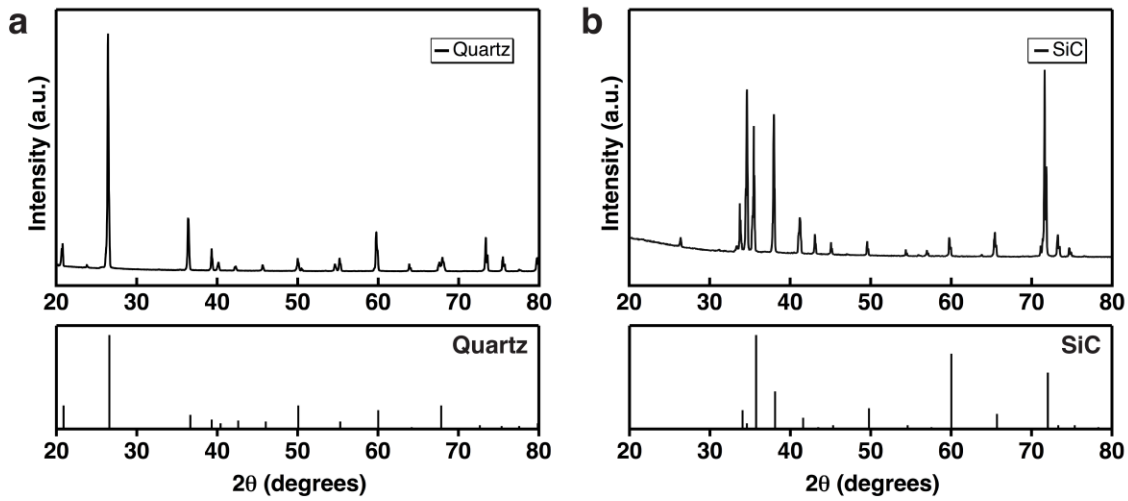

Fig. S12. XRD patterns of (a) quartz and (b) SiC diluent materials with reference diffraction patterns.

Table S3: Analysis of pre- and post- reaction carbon content.

	Pre-reaction carbon (wt%)	Post-reaction carbon (wt%)	Increase in carbon (wt%)
Ni/TiO_2	1.6	4.7	3.1
Ni/Al_2O_3	1.6	5.8	4.2
Ni/MgO	0.8	8.9	8.1
Rh_2P/TiO_2	2.9	6.6	3.8
Rh_2P/Al_2O_3	3.3	12.5	9.2
Rh_2P/MgO	1.4	6.8	5.3

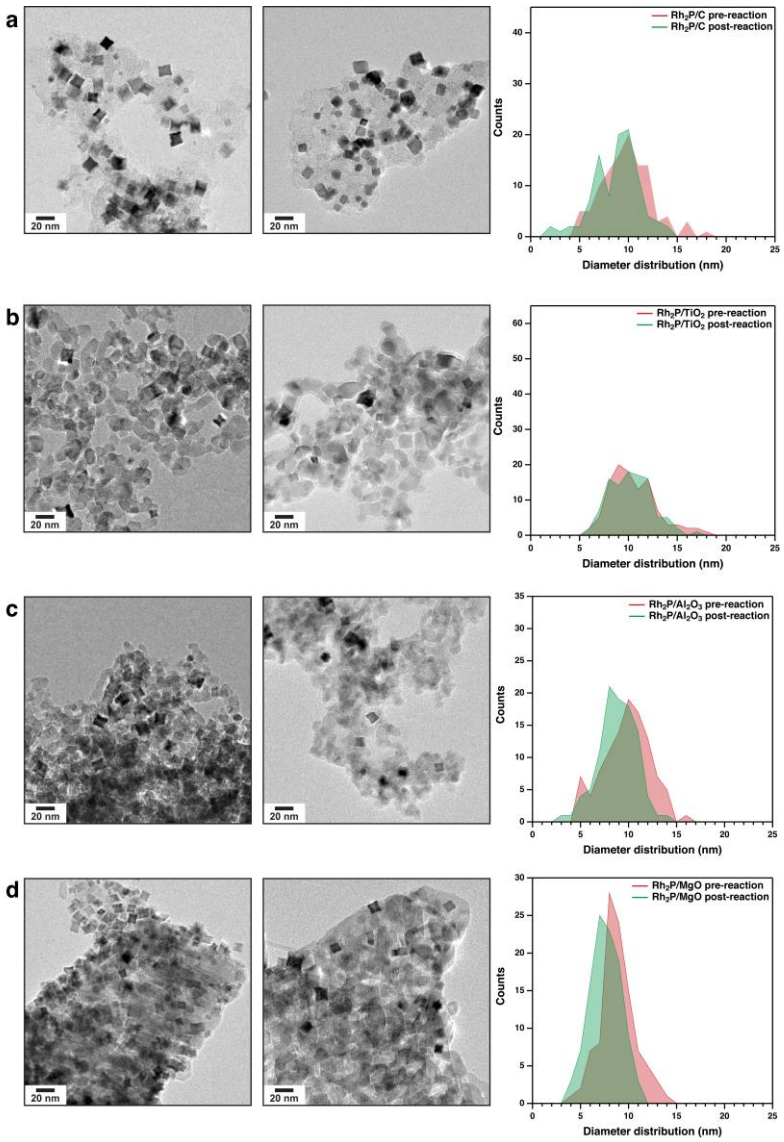

Fig. S13. Pre- (left) and post-reaction (middle) TEM images of (a) Rh_2P/C, (b) Rh_2P/TiO_2, (c) Rh_2P/Al_2O_3, and (d) Rh_2P/MgO with corresponding particle size distributions (right).

Table S4: The surface area weighted average particle size for pre-reaction and post-reaction Ni catalysts as determined by TEM and calculated according to $\left(\frac{\sum D_{P,i}^{3}}{\sum D_{P,i}^{2}}\right)$.

	Pre-reaction (nm)	Post-reaction (nm)
Ni/C	11.6	13.5
Ni/TiO_2	14.6	23.4
Ni/Al_2O_3	11.9	13.4
Ni/MgO	10.7	16.3